ADVANCED MATERIALS

www.advmat.de

Highly Luminescent 2D-Type Slab Crystals Based on a Molecular Charge-Transfer Complex as Promising Organic Light-Emitting Transistor Materials

*Sang Kyu Park, Jin Hong Kim, Tatsuhiko Ohto, Ryo Yamada, Andrew O. F. Jones, Dong Ryeol Whang, Illhun Cho, Sangyoon Oh, Seung Hwa Hong, Ji Eon Kwon, Jong H. Kim, Yoann Olivier, Roland Fischer, Roland Resel, Johannes Gierschner, Hirokazu Tada, and Soo Young Park**

A new 2:1 donor (D):acceptor (A) mixed-stacked charge-transfer (CT) cocrystal comprising isometrically structured dicyanodistyrylbenzene-based D and A molecules is designed and synthesized. Uniform 2D-type morphology is manifested by the exquisite interplay of intermolecular interactions. In addition to its appealing structural features, unique optoelectronic properties are unveiled. Exceptionally high photoluminescence quantum yield ($\Phi_F \approx 60\%$) is realized by non-negligible oscillator strength of the S_1 transition, and rigidified 2D-type structure. Moreover, this luminescent 2D-type CT crystal exhibits balanced ambipolar transport (μ_h and μ_e of $\approx 10^{-4}$ cm^2 V^{-1} s^{-1}). As a consequence of such unique optoelectronic characteristics, the first CT electroluminescence is demonstrated in a single active-layered organic light-emitting transistor (OLET) device. The external quantum efficiency of this OLET is as high as 1.5% to suggest a promising potential of luminescent mixed-stacked CT cocrystals in OLET applications.

Molecular charge-transfer (CT) cocrystals are comprised of regularly stacked electron donor (D) and acceptor (A) constituents that can provoke versatile physical properties – i.e., (super)conductivity,[1] ferroelectricity,[2] photoconductivity,[3] ambipolar transport,[4] and luminescence;[5] based on their peculiar heteromolecular arrangement (segregated-stack or mixed-stack), degree of CT, band filling, and electronic interactions.[6] The intermolecular arrangement and electronic properties of CT crystals are influenced by the primary molecular structures of D and A pairs, which determine their relative molecular orbital (MO) offset as well as types and strengths of intermolecular interaction.[7] Therefore, comprehensive consideration of adequate D–A pair selection is essential to target specific functionalities of CT crystals.

One specific application of mixed-stacked CT complexes, which has been attracting ever increasing research interest in recent years, is the use of them as a new class of ambipolar transporting semiconductors.[4] Molecular orbital interaction within a mixed CT stack has been shown to afford efficient electronic coupling both for holes and electrons via superexchange as revealed from quantum chemical calculations.[8] In addition to the

Dr. S. K. Park, J. H. Kim, Dr. D. R. Whang, Dr. I. Cho, S. Oh, S. H. Hong, Dr. J. E. Kwon, Prof. S. Y. Park
Center for Supramolecular Optoelectronic Materials
Department of Materials Science and Engineering
Seoul National University
1 Gwanak-ro, Gwanak-gu, Seoul 151-744, South Korea
E-mail: parksy@snu.ac.kr

Dr. T. Ohto, Dr. R. Yamada, Prof. H. Tada
Graduate School of Engineering Science
Osaka University
1-3 Machikaneyama, Toyonaka, Osaka 560-8531, Japan

Dr. A. O. F. Jones, Prof. R. Resel
Institute of Solid State Physics
Graz University of Technology
Graz 8010, Austria

Prof. J. H. Kim
Department of Applied Chemistry and Biological Engineering
Department of Molecular Science and Technology
Ajou University
206 Worldcup-ro, Yeongtong-gu, Suwon 443-749, South Korea

Dr. Y. Olivier
Laboratory for Chemistry of Novel Materials
Université de Mons
Place du Parc 20, 7000 Mons, Belgium

Prof. R. Fischer
Institute of Inorganic Chemistry
Graz University of Technology
Graz 8010, Austria

Dr. J. Gierschner
Madrid Institute for Advanced Studies
IMDEA Nanoscience
Calle Faraday 9
Ciudad Universitaria de Cantoblanco
28049 Madrid, Spain

DOI: 10.1002/adma.201701346

peculiar ambipolarity, characteristic CT luminescence and other photonics applications of such D–A compounds are being unveiled,[5] implying potential application of them as organic light-emitting transistor (OLET) based on their combined transport and emission properties, which however is yet to be demonstrated.

We have previously demonstrated that CT luminescence could arise in a 1D-type **CT1** crystal comprising an isometric donor based on distyrylbenzene and an acceptor based on the cyano-substituted variant (dicyanodistyrylbenzene (DCS)), as shown in **Scheme 1**a. **CT1** showed promising ambipolarity (p-channel: 6.7×10^{-3} cm^2 V^{-1} s^{-1}, and n-channel: 6.7×10^{-2} cm^2 V^{-1} s^{-1}) and also high CT photoluminescence quantum yield (PLQY) ($\Phi_F \approx 35\%$).[9] Moreover, loosely packed luminescent **CT2** system based on noncentrosymmetric A_{CT2} material showed stimuli-responsive high-contrast fluorescence switching behavior (Φ_F = 3% and 8% for solvent included and excluded form, respectively), see Scheme 1b.[5e] However, in order to realize OLETs, even higher Φ_F with more balanced ambipolarity is desirable. To this end, 2D-type crystalline morphology, instead of the previously demonstrated and most prevalent 1D-type microwhisker morphology driven by anisotropic CT interactions, is more appropriate. This is because 2D supramolecular factors will not only provide uniform channel coverage with reduced grain boundaries but also will afford uniform interfaces between active layer/dielectric as well as active layer/electrodes.[10]

Herein, we report a new and 2D-type assembling **CT3** system which is capable of both ambipolar charge transport and bright luminescence. The mixed-stacked 2:1 D:A **CT3** complex is

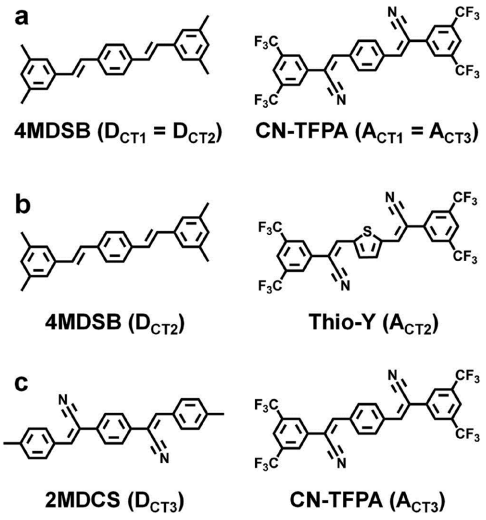

Scheme 1. a–c) Donor and acceptor pairs of **CT1** (a),[9] **CT2** (b),[5e] and **CT3** (c).

based on the DCS motif for the donor (**2MDCS**, D_{CT3}) and the acceptor (**CN-TFPA**, A_{CT3}), as shown in Scheme 1c,[11,12] which establishes in fact a peculiar quasi-2D arrangement based on various in-plane intermolecular interactions; i.e., Coulombic CT and π–π interactions within the mixed-stack CT columns, and side-by-side −CN induced dipole interactions between them. Such intriguing 2D-type supramolecular features, in addition to the highest Φ_F (60%) ever reported for CT crystals and the well-balanced ambipolar transport, suggest this system

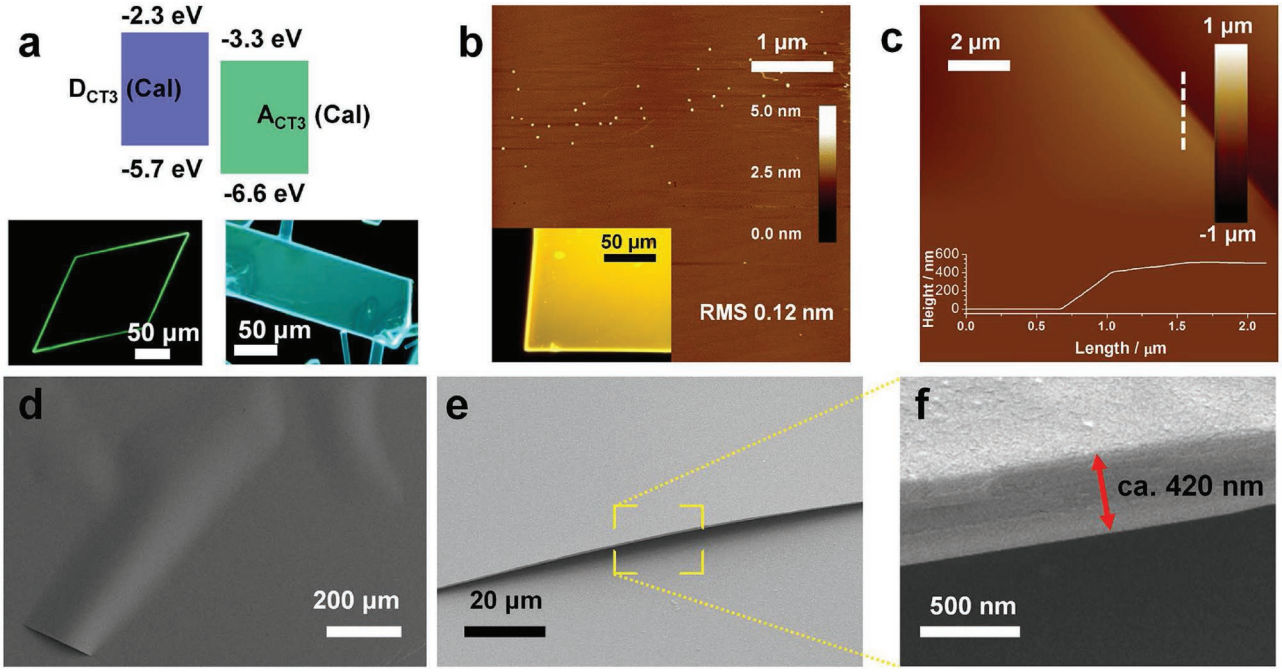

Figure 1. a) DFT (B3LYP, 6-31G(d,p)) calculated frontier molecular orbitals of D_{CT3}, and A_{CT3}. The insets are optical microscopy images for D_{CT3}, and A_{CT3} crystals. b) Atomic force microscopy (AFM) image of **CT3** cocrystal surface. The inset of (b) is an optical microscopy image of PVT-grown **CT3** cocrystal, taken under 365 nm UV irradiation. c) AFM image of thin PVT-grown **CT3** cocrystal with thickness profile. The inset of (c) shows thickness of ≈500 nm, measured along dashed white line. d–f) Field-emission scanning electron microscopy images of PVT-grown 2D-type **CT3** cocrystal exhibiting flexible nature. The red arrow in (f) estimates crystal thickness of ≈420 nm.

for electroluminescence (EL) applications. In fact, we report here the first CT-cocrystal-based high-efficiency OLET device.

Previously, we have proposed the isometric approach to create luminescent CT crystals, by using $\mathbf{D_{CT1}}$ and $\mathbf{A_{CT1}}$ molecules being structurally similar and isometric while electronically complementary to assume a large MO offset (Scheme 1a).[9] This **CT1** pair favored very dense quasi-1D mixed-stack formation, with quite high PLQY, but rather unbalanced ambipolar transport. In order to force the D, A molecules into a 2D-type CT platform with enhanced luminescence, we decided to use a 2D directing supramolecular synthon in both D and A. For this, we introduced the cyano motif also in D, which lowers the energetic MO offset between $\mathbf{D_{CT3}}$ and $\mathbf{A_{CT3}}$ (Scheme 1c and **Figure 1**a). While MO offset between $\mathbf{D_{CT3}}$ and $\mathbf{A_{CT3}}$ is still strong to promote pronounced CT character, its reduction should give rise to the enhanced PL efficiency. In screening the D structure, we varied the steric director, i.e., the position of the methyl-group in the terminal rings of D (para vs meta), as well as the position of the cyano-substituent in the inner/outer (α vs β) vinylene position (see Scheme S1 of the Supporting Information). Among these four possible donors, only $\mathbf{D_{CT3}}$ resulted in cocrystal formation with $\mathbf{A_{CT3}}$ (Scheme 1c), giving a quasi-2D mixed-stacked arrangement of 2:1 stoichiometry with bright emission and ambipolar transport properties. The cocrystals were easily fabricated by physical vapor transport (PVT), see inset of Figure 1b, giving sub-centimeter sized sheets of a few hundred nanometers thickness and high uniformity as analyzed by atomic force microscopy (AFM) (Figure 1b,c, root mean square (RMS) roughness value of 0.12 nm, 5 μm × 5 μm and thickness of ≈500 nm). The characteristic thickness renders a favorable flexibility (Figure 1d,e).[13] The thickness of the 2D-type crystals in Figure 1e was estimated to be 420 nm, see Figure 1f. The molecular arrangement in **CT3** gives rise to evident charge-transfer in the ground state as revealed by electron spin resonance analysis, yielding a *g*-factor value of 2.0082, see Figure S1 (Supporting Information). Mulliken atom charge analysis based on density functional theory (DFT) calculations indeed reveals weak ground state CT, see Figure S2 (Supporting Information).

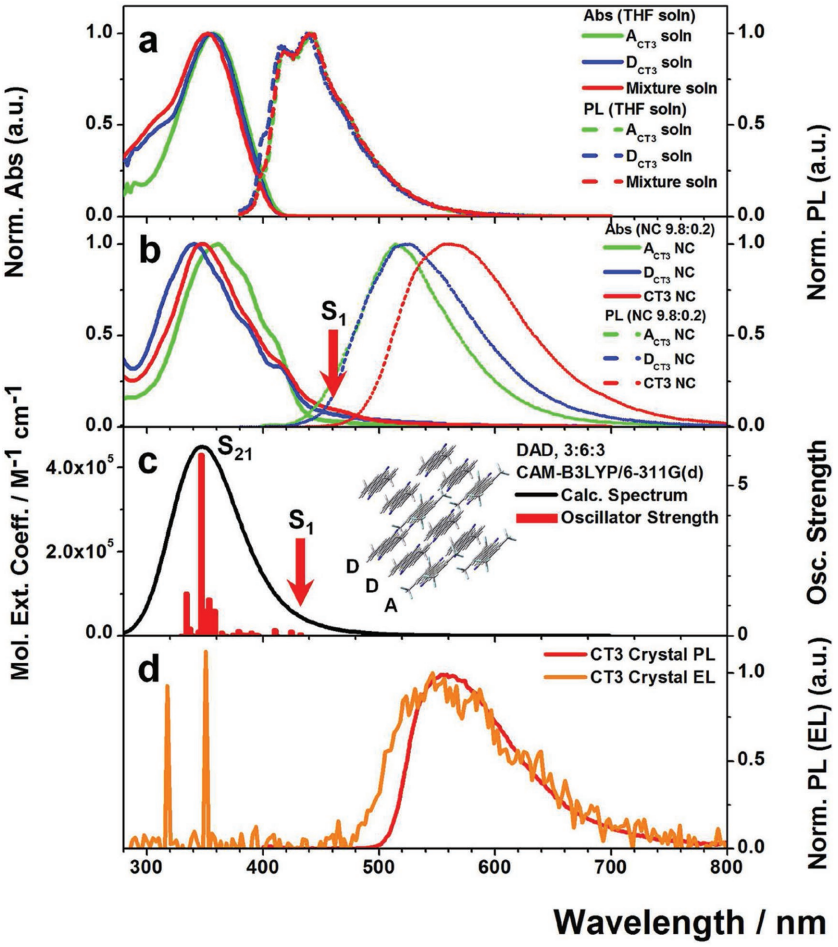

Figure 2. a) Normalized UV–vis absorption (solid lines) and PL (dotted lines) spectra of dilute $\mathbf{D_{CT3}}$, $\mathbf{A_{CT3}}$, and 2:1 $\mathbf{D_{CT3}}$:$\mathbf{A_{CT3}}$ THF solution. b) Normalized UV–vis absorption and PL spectra of $\mathbf{D_{CT3}}$, $\mathbf{A_{CT3}}$, and 2:1 $\mathbf{D_{CT3}}$:$\mathbf{A_{CT3}}$ **CT3** nanocrystals (NC, water:THF, 0.98:0.02). c) DFT calculated UV–vis absorption spectrum and oscillator strength; S_1 and S_{21} transition is indicated in spectrum. The inset of (c): structure of **DDA**, 3-6-3 assembly. d) PL of PVT-grown **CT3** crystal (red solid line), and EL of single-crystal OLET (orange solid line). The PL spectra in each state were obtained by excitation with the absorption maximum in the corresponding state. The excitation wavelengths are indicated in parentheses: $\mathbf{A_{CT3}}$ Soln (358 nm), $\mathbf{D_{CT3}}$ Soln (357 nm), Mixture Soln (352 nm), $\mathbf{A_{CT3}}$ NC (360 nm), $\mathbf{D_{CT3}}$ NC (341 nm), **CT3** NC (350 nm), and **CT3** crystal (350 nm).

UV–vis absorption and PL spectra of **CT3** nanocrystals (NC, fabricated in tetrahydrofuran (THF):H_2O = 2:98, v:v) are shown in **Figure 2**, along with the $\mathbf{D_{CT3}}$ and $\mathbf{A_{CT3}}$ solution spectra and the PL spectrum of a PVT-grown **CT3** crystal. As in **CT1** and **CT2** nanocrystals reported before, the absorption spectrum of **CT3** nanocrystals exhibits a strongly red-shifted absorption band (λ_{abs} = 455 nm, S_1 of Figure 2b) of low intensity,[5e,9] which is assigned to a CT transition, giving rise to a broad PL spectrum (λ_{em} = 555 nm). The corresponding PL spectrum of the PVT-grown crystal peaks at the same wavelength, however suffers from some reabsorption. The Φ_F of the PVT-grown single crystal gives about 60%, being a record value for CT crystals reported so far. For the nanocrystals, Φ_F is significantly lower, i.e., 18%, due to the higher exciton trap density by higher surface-to-volume ratio of the ≈100 nm nanocrystals (see Figure S3 of the Supporting Information) compared to the monolithic ≈3 mm-size crystals used for the PL measurements.[9b,14] Such exciton traps can be, e.g., structural imperfection at grain boundaries/surface, chemical impurities, oxygen, etc.[14a]

To gain insight into the CT properties of the cocrystal based on their exact crystalline structure, we carried out single-crystal

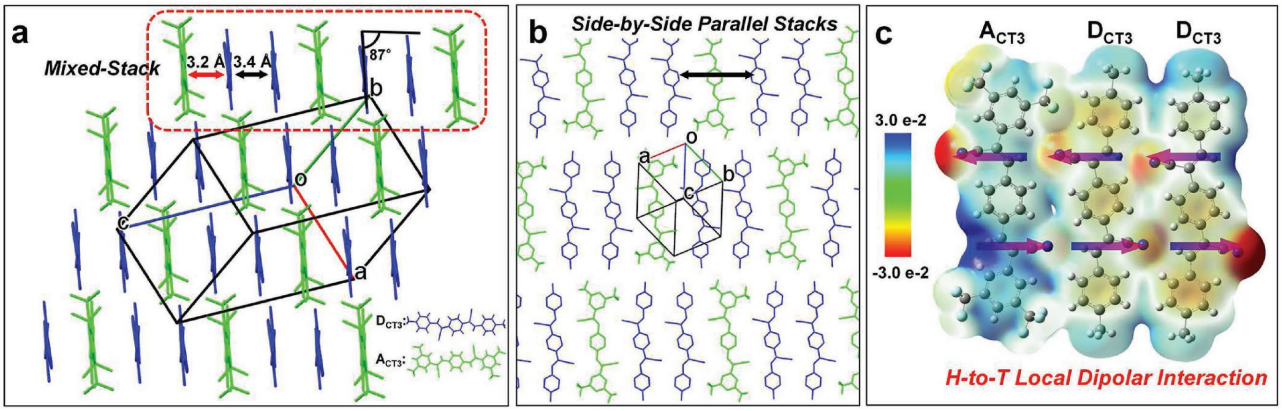

Figure 3. Molecular arrangement in **CT3** cocrystal found from single-crystal XRD; along a) roll angle, and b) π-facet view. Distance between $\mathbf{D_{CT3}}$–$\mathbf{A_{CT3}}$ (red arrow), and $\mathbf{D_{CT3}}$–$\mathbf{D_{CT3}}$ (black arrow) as well as counter roll angle (87°) are indicated within a mixed-stack (red-dotted box) in (a). The black arrow in (b) indicates side-by-side parallel stacks direction. c) DFT-calculated (B3LYP, 6-31G(d,p)) electrostatic potential map, manifesting head-to-tail dipolar interaction induced from —CN functionalities.

X-ray diffraction (SC-XRD) analysis as shown in **Figure 3** and also in Table S1 and Figure S4 (Supporting Information). The $\mathbf{D_{CT3}}$ and $\mathbf{A_{CT3}}$ molecules are tightly stacked in a 2:1 $\mathbf{D_{CT3}}$:$\mathbf{A_{CT3}}$ mixed-stack arrangement (Figure 3a) through intermolecular CT interaction. At the same time, these 1D-type CT stacks are further linked side-by-side (Figure 3b) to give quasi-2D-type sheets of $\mathbf{D_{CT3}}$–$\mathbf{D_{CT3}}$–$\mathbf{A_{CT3}}$ motif. Such 2D-type assembling features can be attributed to notable in-plane secondary interactions; i.e., π–π and CT interactions within the mixed-stack, and head-to-tail dipolar interactions of the cyano groups between the parallel stacks. The latter is clearly observed in the electrostatic potential map as shown in Figure 3c. The separation between neighboring molecules in the mixed-stack is ≈3.2 and ≈3.4 Å for $\mathbf{D_{CT3}}$–$\mathbf{A_{CT3}}$ and $\mathbf{D_{CT3}}$–$\mathbf{D_{CT3}}$, respectively; and the counter roll angle is 87°, giving in all favorable MO overlap within the stack (Figure 3a).

Based on the crystal structure, we carried out time-dependent DFT (TD-DFT) calculations using the long-range corrected CAM-B3LYP functional, of which the results are shown in Figure S5 (Supporting Information). Due to the 2D-type stacking character, a noticeable size dependency of the excited state energies is found as expected (Figure S5 and S6, Supporting Information), and thus we had to calculate a larger assembly, i.e., a 3-6-3 cluster, (see inset of Figure 2c) to well reproduce the measured absorption properties (Figure 2b). The main absorption is assigned to a $\mathbf{D_{CT3}}$-localized transition (S_{21}), while the lowest excited state (S_1) indeed reveals clear CT character, which affords a non-negligible oscillator strength ($f = 0.05$) due to a small locally excited character contribution found from natural transition orbital analysis (Figure S7, Supporting Information). This agrees quite well with experimental value of $f = 0.15$ (Figure S8, Supporting Information). It should be stressed that the CT character and thus the energetic stabilization of S_1 is significantly smaller compared to those in the **CT1** system.[9] This is due to the fact that both $\mathbf{D_{CT3}}$ and $\mathbf{A_{CT3}}$ are of DCS-type in the **CT3** system, while it was the case only for the acceptor in the **CT1** system. Importantly, the non-negligible S_1–S_0 oscillator strength of $f = 0.15$ gives rise to a considerable radiative rate, calculated by $k_F = \Phi_F/\tau_F = 2.3 \times 10^7\ s^{-1}$ (**Table 1** and Figure S9 (Supporting Information)). At the same time, low nonradiative rate of $k_{nr} = 1.5 \times 10^7\ s^{-1}$ was found, which is ascribed mainly to the dense packing and the rigidified structure in the 2D-type stack.

The charge-transport properties were first evaluated in a single-crystal OFET (SC-OFET) with staggered device geometry, using PVT-grown thin **CT3** crystals (thickness of ≈200–500 nm). Because of flexible feature of PVT-grown thin **CT3** crystals, conformal contact was available during lamination procedure. The top Au-contact SC-OFETs manifest distinct V-shape transfer characteristics as well as peculiar ambipolar output characteristics (changing from superlinear to saturation behavior upon increasing gate bias $|V_G|$), as shown in Figure S10a–d (Supporting Information). As seen in **Table 2**, the device exhibited highly balanced ambipolar transport (p-channel: 5.5×10^{-4} and

Table 1. Summarized optical characteristics of $\mathbf{D_{CT3}}$, $\mathbf{A_{CT3}}$, and **CT3** cocrystal.

	$\lambda_{abs,S1}$ [a] [nm]	ε_m [b] [$10^4\ M^{-1}\ cm^{-1}$]	$f_{exp,CT}$ [c]	$f_{cal,CT}$ [d]	λ_{em} [e] [nm]	Φ_F	$\tau_{F,Avg}$ [ns]	k_F [f] [$\times 10^7\ s^{-1}$]	k_{nr} [g] [$\times 10^7\ s^{-1}$]
$\mathbf{D_{CT3}}$	340	2.38	–	–	526	0.89	3.3	27.0	3.3
$\mathbf{A_{CT3}}$	361	3.90	–	–	514	0.83	6.3	13.2	2.7
CT3	455	1.14	0.15	0.05	555	0.60	26.3	2.3	1.5

[a]Absorption maximum wavelength for nanocrystals suspensions of constituents ($\mathbf{D_{CT3}}$ and $\mathbf{A_{CT3}}$), and wavelength for S_1 transition in **CT3** nanocrystals suspensions; [b]Molar extinction coefficient derived from absorption spectra of nanocrystals; [c]Experimentally extracted oscillation strength for **CT3** nanocrystals; [d]TD-DFT calculated oscillation strength from 3-6-3 cluster; [e]PL maximum wavelength; [f]Radiative rates calculated by $\Phi_F/\tau_{F,Avg}$; [g]Nonradiative rates calculated by $(1 - \Phi_F)/\tau_{F,Avg}$.

Table 2. Summarized transistors characteristics of **CT3** cocrystal.

		μ_{max} [a)] [$cm^2 V^{-1} s^{-1}$]	μ_{avg} [a)] [$cm^2 V^{-1} s^{-1}$]	V_T [b)] [V]	On/off	n [c)]
Top Au-contact	p	5.5×10^{-4}	2.5×10^{-4}	–54	10^2–10^3	10
	n	2.9×10^{-4}	1.5×10^{-4}	55	10^1–10^3	10
Top Al-contact	p [d)]	–	–	–	–	–
	n	9.0×10^{-4}	7.0×10^{-4}	42	10^2–10^3	10
Top MoOx/Ag-contact	p	4.2×10^{-3}	1.3×10^{-3}	–54	10^3–10^5	10
	n	7.2×10^{-4}	4.2×10^{-4}	15	10^1–10^3	10
Bottom Au-contact	p	1.8×10^{-5}	9.2×10^{-6}	5	10^1–10^2	4
	n	4.9×10^{-5}	2.7×10^{-5}	30	10^1–10^3	4

[a)]The mobility values for hole (electron) are extracted from the saturation regime of the p-channel (n-channel) carrier enhancement mode; [b)]Average threshold voltage; [c)]Number of devices; [d)]Top Al-contact SC-OFETs do not show p-channel transistors characteristics.

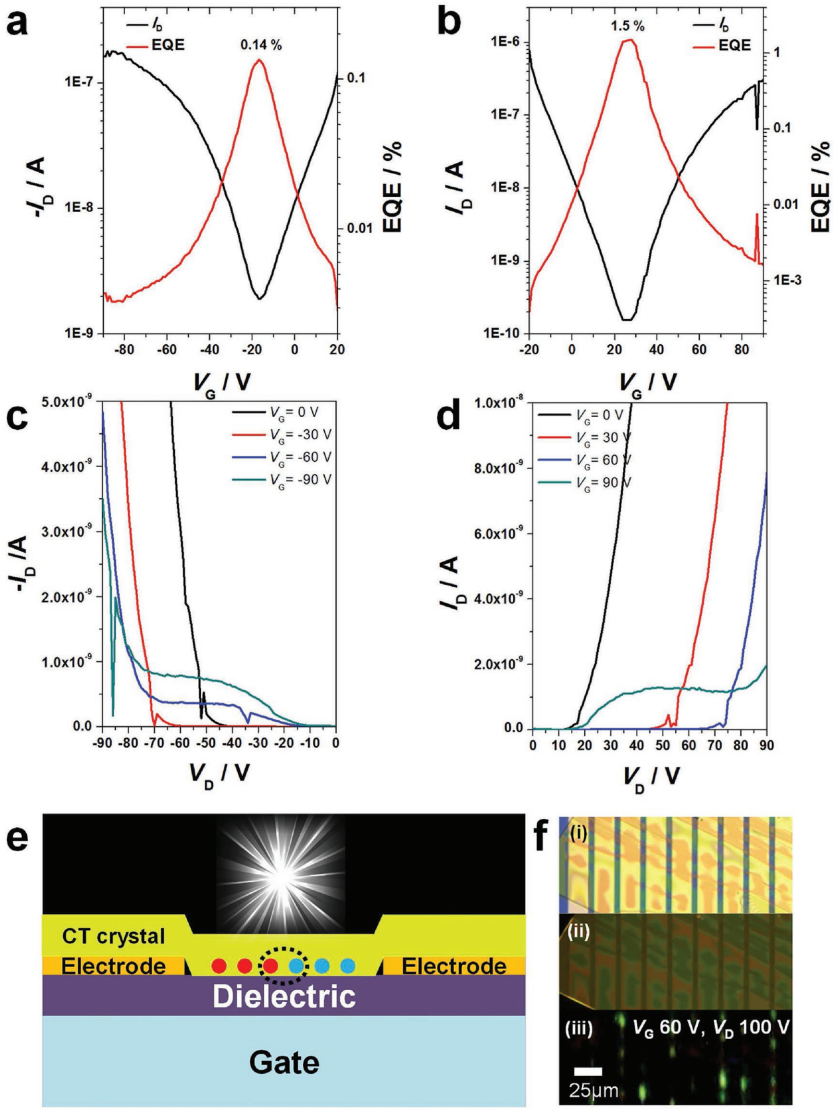

Figure 4. a,b) p-channel and n-channel transfer characteristics (black line) and external quantum efficiency (red line). c,d) p-channel and n-channel output characteristics. e) Schematic illustration for the bottom-contact SC-OLET device. f) Images of a device; taken by optical microscopy under white light irradiation (i) and UV irradiation (ii). (iii) was captured during device operation (constant bias condition, V_G: 60 V, V_D: 100 V).

n-channel: 2.9×10^{-4} cm^2 V^{-1} s^{-1}). The somewhat low mobility is attributed to the high ionization energy = 5.9 eV and low electron affinity = 3.7 eV of the cocrystal with respect to the work function of Au (≈4.9 eV),[15] bringing about a large contact resistance due to the charge injection barrier (see Figure S11 of the Supporting Information). This is evident from the sublinear current increase in the small V_D regime of the output characteristics as shown in Figure S10c,d (Supporting Information). Indeed, devices with a different source–drain contact (MoO_3/Ag) render enhanced mobilities, or even unipolar n-channel property (case of top Al contact) without severe contact resistance, as shown in Figure S10e–h (Supporting Information) and Table 2. The top Au-contact devices show a threshold voltage hysteresis (ΔV_T) of about 12 V in both hole and electron enhancement modes, due to the remaining traps at the surface of octadecyltrichlorosilane (ODTS) treated SiO_2, see Figure S12a,b (Supporting Information). The influence of such traps on ΔV_T can be further reduced by employing a polystyrene passivation layer (100 nm), giving ΔV_T of about 5–6 V and increased mobility, see Figure S12e,f (Supporting Information).

The balanced bipolar transport and high Φ_F indicate the possibility for realizing EL in an OLET device.[16,17] For the simplicity of photocurrent and EL spectrum measurement, Au prepatterned bottom-contact bottom-gate device geometry was utilized, where the channel length was 5 µm fabricated by photolithography. As in the case of top-contact devices, flexible PVT-grown **CT3** crystals were laminated on to the source/drain electrodes, as shown in **Figure 4**e. The AFM image in Figure S13a (Supporting Information) reveals similar thickness between electrode and substrate ($t \approx 30$ nm) and height difference in crystal adhered to this border ($t \approx 30$ nm), which supports a good dielectric–crystal interface quality. In addition, the cross-section of the device was analyzed with transmission electron microscopy (TEM) (Figure S13b,c, Supporting Information; seperately prepared 2 µm thick

CT3 samples were used), which also exhibits conformal contact. Like in the top-contact configuration, the devices render apparent V-shape transfer and ambipolar output characteristics as shown in Figure 4a–d. The hysteresis of the typical bottom Au-contact device was also investigated, whose electrodes were formed by vacuum deposition through a shadow mask, see Figure S12c,d (Supporting Information). EL is clearly exhibited during OLET device operation as shown in Figure 4f, which was imaged during constant bias condition using a microscope connected to a charge-coupled device (CCD) camera. The light emission appears to cover the 5 μm channel region between source–drain electrodes. The EL spectrum virtually coincides with the PL characteristic from **CT3** (nano)crystals (Figure 2b,d), which indicates that CT excitons of S_1 state are generated by bipolar charge carrier injection into the luminescent CT crystal. While OLET devices employing p-/n-channel heterostructures (i.e., multilayer, planar, and bulk heterojunctions) have frequently been reported,[17] we herein report the first example of CT-complex-based SC-OLET. Moreover, the external quantum efficiency (EQE) of our CT device reached as high as 1.5% from the n-channel enhancement mode (see Figure 4b). It was observed that both p-/n-channel enhancement modes showed EQE maxima at drain current minima, which mainly ascribed to the reduced exciton quenching at the electrodes and exciton–polaron annihilation. It is noteworthy that the EQE of 1.5% is among the highest values observed from single-layer active-channel OLET devices (in general EQE <1% for the top-emitting devices,[16g,h] EQE >8% in the bottom-emitting device with an adequate optical cavity).[16] Such encouraging results can be attributed to the high Φ_F and favorable bipolar carrier injection/transport of the **CT3** system.

In conclusion, we have designed and fabricated a novel 2:1 D:A mixed-stack CT system with 2D-type stacking nature. Unique 2D-type assembly of the complementary $\mathbf{D_{CT3}}$–$\mathbf{A_{CT3}}$ pair was promoted by head-to-tail dipolar −CN alignment, which resulted in a highly uniform and flexible 2D-type supramolecular structure. Interestingly, this 2D-type assembling feature significantly affects photophysical property as revealed from TD-DFT calculation, and presumably leads to ambipolar characteristic within 2:1 D:A stoichiometry. In virtue of bright luminescence ($\Phi_F \approx 60\%$) and ambipolar transport (μ_h and μ_e of $\approx 10^{-4}$ cm^2 V^{-1} s^{-1}) of this **CT3** system, we could demonstrate the first CT-cocrystal-based OLET device which exhibited EQE as high as 1.5% in the pristine device structure. The **CT3** presented in this report provide important insight on tailoring supramolecular/optoelectronic properties of intermolecular CT systems, and shed light on the possibilities of luminescent CT as active materials for future lighting applications.

CCDC 1520198 contains the supplementary crystallographic data for this paper. These data can be obtained free of charge from The Cambridge Crystallographic Data Centre via www.ccdc.cam.ac.uk/data_request/cif.

Supporting Information

Supporting Information is available from the Wiley Online Library or from the author.

Acknowledgements

The research from the Seoul National University was supported by the National Research Foundation of Korea (NRF) through a grant funded by the Korean government (MSIP; No. 2009-0081571[RIAM0417-20150013]) and the Global Frontier R&D Program on Center for Multiscale Energy System funded by the NRF under the MSIP, Korea (2012M3A6A7055540). The spectroscopic and computational work at the IMDEA was performed in the context of the European COST Action Nanospectroscopy, MP1302. Financial support at the IMDEA was provided by the Spanish Ministerio de Economía y Competitividad (project CTQ2014-58801), by the Comunidad de Madrid (Project Mad2D, Grant No. S2013/MIT-3007) and by the Campus of International Excellence (CEI) UAM+CSIC. The research from the Osaka University was partly supported by the Osaka–Seoul Joint Research Promotion Program, Osaka University. J.G. thanks Begoña Milián-Medina (Valencia, Spain) for helpful discussions.

Conflict of Interest

The authors declare no conflict of interest.

Keywords

2D, ambipolar transport, charge-transfer complexes, luminescence, organic light-emitting transistors

Received: March 9, 2017
Revised: April 22, 2017
Published online: July 26, 2017

[1] a) J. Ferraris, D. O. Cowan, V. Walatka, J. H. Perlstein, *J. Am. Chem. Soc.* **1973**, *95*, 948; b) D. Jérome, A. Mazaud, M. Ribault, K. Bechgaard, *J. Phys. Lett.* **1980**, *41*, 95.

[2] a) Y. Tokura, S. Koshihara, Y. Iwasa, H. Okamoto, T. Komatsu, T. Koda, N. Iwasawa, G. Saito, *Phys. Rev. Lett.* **1989**, *63*, 2405; b) A. S. Tayi, A. K. Shveyd, A. C.-H. Sue, J. M. Szarko, B. S. Rolczynski, D. Cao, T. J. Kennedy, A. A. Sarjeant, C. L. Stern, W. F. Paxton, W. Wu, S. K. Dey, A. C. Fahrenbach, J. R. Guest, H. Mohseni, L. X. Chen, K. L. Wang, J. F. Stoddart, S. I. Stupp, *Nature* **2012**, *488*, 485; c) S. Chen, X. C. Zeng, *J. Am. Chem. Soc.* **2014**, *136*, 6428.

[3] a) J. Tsutsumi, T. Yamada, H. Matsui, S. Haas, T. Hasegawa, *Phys. Rev. Lett.* **2010**, *105*, 226601; b) W. Yu, X.-Y. Wang, J. Li, Z.-T. Li, Y.-K. Yan, W. Wang, J. Pei, *Chem. Commun.* **2013**, *49*, 54.

[4] a) J. Zhang, H. Geng, T. S. Virk, Y. Zhao, J. Tan, C.-a. Di, W. Xu, K. Singh, W. Hu, Z. Shuai, Y. Liu, D. Zhu, *Adv. Mater.* **2012**, *24*, 2603; b) J. Zhang, J. Tan, Z. Ma, W. Xu, G. Zhao, H. Geng, C. Di, W. Hu, Z. Shuai, K. Singh, D. Zhu, *J. Am. Chem. Soc.* **2013**, *135*, 558; c) Y. Qin, J. Zhang, X. Zheng, H. Geng, G. Zhao, W. Xu, W. Hu, Z. Shuai, D. Zhu, *Adv. Mater.* **2014**, *26*, 4093; d) D. Vermeulen, L. Y. Zhu, K. P. Goetz, P. Hu, H. Jiang, C. S. Day, O. D. Jurchescu, V. Coropceanu, C. Kloc, L. E. McNeil, *J. Phys. Chem. C* **2014**, *118*, 24688; e) Y. Qin, C. Cheng, H. Geng, C. Wang, W. Hu, W. Xu, Z. Shuai, D. Zhu, *Phys. Chem. Chem. Phys.* **2016**, *18*, 14094.

[5] a) W. Zhu, R. Zheng, Y. Zhen, Z. Yu, H. Dong, H. Fu, Q. Shi, W. Hu, *J. Am. Chem. Soc.* **2015**, *137*, 11038; b) Y.-L. Lei, Y. Jin, D.-Y. Zhou, W. Gu, X.-B. Shi, L.-S. Liao, S.-T. Lee, *Adv. Mater.* **2012**, *24*, 5345; c) W. Zhu, R. Zheng, X. Fu, H. Fu, Q. Shi, Y. Zhen, H. Dong, W. Hu, *Angew. Chem., Int. Ed.* **2015**, *54*, 6785; d) W. Zhu, L. Zhu, Y. Zou, Y. Wu, Y. Zhen, H. Dong, H. Fu, Z. Wei, Q. Shi, W. Hu, *Adv. Mater.*

2016, *28*, 5954; e) S. K. Park, I. Cho, J. Gierschner, J. H. Kim, J. H. Kim, J. E. Kwon, O. K. Kwon, D. R. Whang, J.-H. Park, B.-K. An, S. Y. Park, *Angew. Chem., Int. Ed.* **2016**, *55*, 203.

[6] a) G. Saito, T. Murata, *Philos. Trans. R. Soc., A* **2008**, *366*, 139; b) T. Mori, *Chem. Rev.* **2004**, *104*, 4947.

[7] F. H. Herbstein, *Crystalline Molecular Complexes and Compounds: Structures and Principles*, Oxford University Press, Oxford, UK/New York **2005**.

[8] a) L. Zhu, Y. Yi, Y. Li, E.-G. Kim, V. Coropceanu, J.-L. Brédas, *J. Am. Chem. Soc.* **2012**, *134*, 2340; b) H. Geng, X. Zheng, Z. Shuai, L. Zhu, Y. Yi, *Adv. Mater.* **2015**, *27*, 1443.

[9] a) S. K. Park, S. Varghese, J. H. Kim, S.-J. Yoon, O. K. Kwon, B.-K. An, J. Gierschner, S. Y. Park, *J. Am. Chem. Soc.* **2013**, *135*, 4757; b) M. Wykes, S. K. Park, S. Bhattacharyya, S. Varghese, J. E. Kwon, D. R. Whang, I. Cho, R. Wannemacher, L. Lüer, S. Y. Park, J. Gierschner, *J. Phys. Chem. Lett.* **2015**, *6*, 3682.

[10] a) Y. Shibata, J. Tsutsumi, S. Matsuoka, K. Matsubara, Y. Yoshida, M. Chikamatsu, T. Hasegawa, *Appl. Phys. Lett.* **2015**, *106*, 143303; b) D. Sarkar, X. Xie, W. Liu, W. Cao, J. Kang, Y. Gong, S. Kraemer, P. M. Ajayan, K. Banerjee, *Nature* **2015**, *526*, 91; c) S. D. Wang, T. Miyadera, T. Minari, Y. Aoyagi, K. Tsukagoshi, *Appl. Phys. Lett.* **2008**, *93*, 043311; d) G. Schweicher, Y. Olivier, V. Lemaur, Y. H. Geerts, H. Ma, H.-L. Yip, F. Huang, A. K.-Y. Jen, *Adv. Funct. Mater.* **2010**, *20*, 1371.

[11] a) G. P. Bartholomew, X. Bu, G. C. Bazan, *Chem. Mater.* **2000**, *12*, 2311; b) S.-J. Lim, B.-K. An, S. Y. Park, *Macromolecules* **2005**, *38*, 6236.

[12] a) S. K. Park, J. H. Kim, S.-J. Yoon, O. K. Kwon, B.-K. An, S. Y. Park, *Chem. Mater.* **2012**, *24*, 3263; b) S. Varghese, S. K. Park, S. Casado, R. Resel, R. Wannemacher, L. Lüer, S. Y. Park, J. Gierschner, *Adv. Funct. Mater.* **2016**, *26*, 2349.

[13] A. L. Briseno, R. J. Tseng, M.-M. Ling, E. H. L. Falcao, Y. Yang, F. Wudl, Z. Bao, *Adv. Mater.* **2006**, *18*, 2320.

[14] a) J. Gierschner, L. Lüer, B. Milián-Medina, D. Oelkrug, H.-J. Egelhaaf, *J. Phys. Chem. Lett.* **2013**, *4*, 2686; b) J. Gierschner, S. Y. Park, *J. Mater. Chem. C* **2013**, *1*, 5818.

[15] a) X. Cheng, Y.-Y. Noh, J. Wang, M. Tello, J. Frisch, R.-P. Blum, A. Vollmer, J. P. Rabe, N. Koch, H. Sirringhaus, *Adv. Funct. Mater.* **2009**, *19*, 2407; b) C. Liu, Y. Xu, Y.-Y. Noh, *Mater. Today* **2015**, *18*, 79.

[16] a) F. Cicoira, C. Santato, *Adv. Funct. Mater.* **2007**, *17*, 3421; b) A. Hepp, H. Heil, W. Weise, M. Ahles, R. Schmechel, H. von Seggern, *Phys. Rev. Lett.* **2003**, *91*, 157406; c) J. S. Swensen, C. Soci, A. J. Heeger, *Appl. Phys. Lett.* **2005**, *87*, 253511; d) Z. Zaumseil, R. H. Friend, H. Sirringhaus, *Nat. Mater.* **2006**, *5*, 69; e) S. Hotta, T. Yamao, S. Z. Bisri, T. Takenobu, Y. Iwasa, *J. Mater. Chem. C* **2014**, *2*, 965; f) H. Nakanotani, R. Kabe, M. Yahiro, T. Takenobu, Y. Iwasa, C. Adachi, *Appl. Phys. Express* **2008**, *1*, 091801; g) T. Oyamada, C.-H. Chang, T.-C. Chao, F.-C. Fang, C.-C. Wu, K.-T. Wong, H. Sasabe, C. Adachi, *J. Phys. Chem. C* **2007**, *111*, 108; h) J. Zaumseil, C. R. McNeill, M. Bird, D. L. Smith, P. P. Ruden, M. Roberts, M. J. McKiernan, R. H. Friend, H. Sirringhaus, *J. Appl. Phys.* **2008**, *103*, 064517; i) M. C. Gwinner, D. Kabra, M. Roberts, T. J. K. Brenner, B. H. Wallikewitz, C. R. McNeill, R. H. Friend, H. Sirringhaus, *Adv. Mater.* **2012**, *24*, 2728; j) C. Zhang, P. Chen, W. Hu, *Small* **2016**, *12*, 1252.

[17] a) M. A. Loi, C. Rost-Bietsch, M. Murgia, S. Karg, W. Riess, M. Muccini, *Adv. Funct. Mater.* **2006**, *16*, 41; b) F. Dinelli, R. Capelli, M. A. Loi, M. Murgia, M. Muccini, A. Facchetti, T. J. Marks, *Adv. Mater.* **2006**, *18*, 1416; c) R. Capelli, S. Toffanin, G. Generali, H. Usta, A. Facchetti, M. Muccini, *Nat. Mater.* **2010**, *9*, 496; d) J. H. Kim, A. Watanabe, J. W. Chung, Y. Jung, B.-K. An, H. Tada, S. Y. Park, *J. Mater. Chem.* **2010**, *20*, 1062; e) T. Oyamada, H. Uchiuzou, S. Akiyama, Y. Oku, N. Shimoji, K. Matsushige, H. Sasabe, C. Adachi, *J. Appl. Phys.* **2005**, *98*, 074 506; f) H. Nakanotani, M. Saito, H. Nakamura, C. Adachi, *Adv. Funct. Mater.* **2010**, *20*, 1610.